2022 ACWE 14th Americas Conference on Wind Engineering
May 17-19, 2022 – Lubbock, TX
National Wind Institute – Texas Tech University

Effect of solar panel support structure on the wind loading of horizontal single-axis trackers

Jubayer Chowdhury [a], Heather Sauder [b], David Banks [c]

[a] *CPP Wind Engineering Consultants, Windsor, Colorado, USA, jchowdhury@cppwind.com*
[b] *CPP Wind Engineering Consultants, Windsor, Colorado, USA, hsauder@cppwind.com*
[c] *CPP Wind Engineering Consultants, Windsor, Colorado, USA, dbanks@cppwind.com*

ABSTRACT: Horizontal single-axis trackers (HSATs) are susceptible to wind induced damages and wind loading on these solar trackers is one of the major considerations in their design. HSATs typically feature either a torque tube or dual-rail support structure protruding 0.1 m to 0.2 m below the plane of the PV panels. This study investigates the effect of these protrusions on critical wind-induced loads on these trackers. Wind tunnel tests have been performed for a generic HSAT system for tilts from 0° (flat, horizontal) up to 60° and a full range of wind azimuths. We examine three load cases (tracker wing moment, post normal force and purlin moment) representing a wide range of tributary areas. Significantly increased moments particularly at low tilts, were observed for the configuration with the underneath structures compared to without, indicating the importance of modelling the aerodynamic impact of these structural components when measuring design wind loads for HSATs.

KEYWORDS: Solar, photovoltaic, trackers, torque tube, dual-rail, wind load.

1 INTRODUCTION

Solar trackers follow the path of the sun to maximize the electrical output from the photovoltaic (PV) panels. Horizontal single-axis tracker (HSAT) is one such tracker with one degree of freedom that moves from East in the morning to West in the evening. Most common HSAT design is based on a single torque tube with long axis running in North-South direction at the center of the chord underneath the PV panels. Other types of designs include dual rails close to the top and bottom edge of PV panels instead of a torque tube (Figure 1).

Several load cases need to be investigated for designing HSAT for the wind. Some of these load cases are full-tracker and tracker wing moments, post normal force, purlin moment, module normal force and moment, and clip normal force. These load cases are essential for designing different components of HSAT, such as torque-tube, drive system, post, purlin, and clip, among many others (Figure 2). Two of the most important load cases are full tracker or tracker wing moment and post normal force, as these two load cases are responsible for the design of the torque tube or dual rails which can often be the most expensive structural component of the tracker.

Moments and normal forces for different load cases are usually presented in a non-dimensional form or coefficients to be aligned with different building code standards around the world, such as ASCE 7 (ASCE 7-16, 2017). The normal force coefficient (GC_N) and moment coefficient (GC_M) are defined as:

$$GC_N = \frac{F_N}{q_Z A_{ref}} \tag{1}$$

$$GC_M = \frac{M}{q_Z A_{ref} L} \quad (2)$$

where F_N is the normal force acting on a certain area, M is the moment (either on a purlin, tracker wing or a complete tracker span), q_Z is the reference velocity wind pressure (in this study it is based on 3-second gust speed at a height of 10 m (33 ft) above grade in ASCE 7), A_{ref} represents the reference area, or the tributary area of the modules to which the load applies, and L represents the chord length.

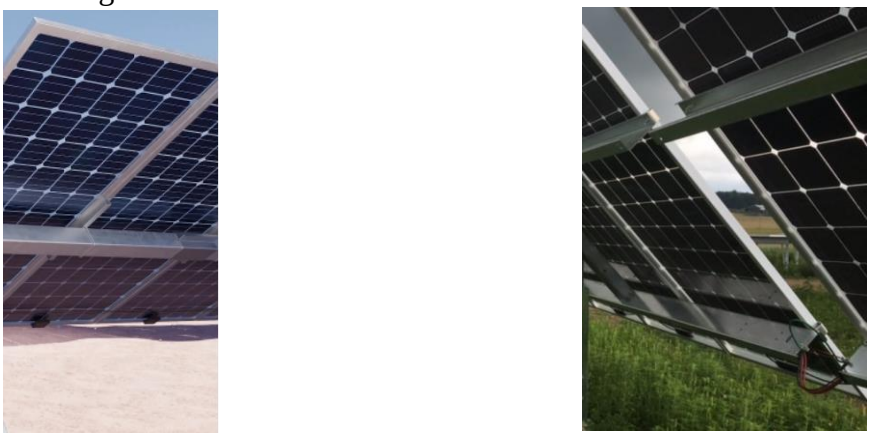

Torque tube Dual-rail

Figure 1. HSAT systems with torque tube and dual-rail (images taken from solarpowerworldonline.com)

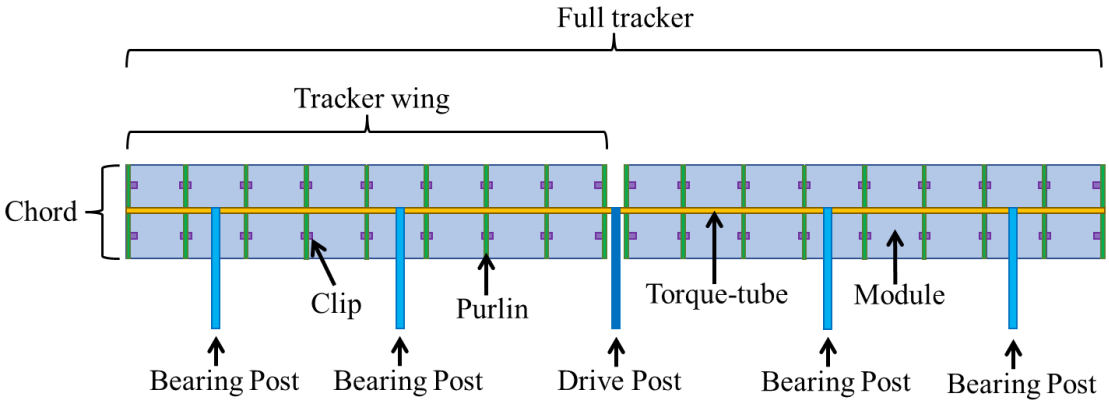

Figure 2. Some of the components of a HSAT system with a torque tube

According to the wind tunnel testing standards by ASCE (ASCE/SEI 49-21, 2021), architectural details that extend 2% or more of the least horizontal dimension in full-scale should be included in the wind tunnel model. Typical torque tube or dual rails protrudes by about 0.1 m to 0.2 m, which is more than 2% for a generic tracker system with one-in-portrait modules. The goal of the present study is to investigate the effect of these support structures (torque tube and dual-rails) on the wind loading of HSATs. To fulfill the objectives of the present study, a series of tests was conducted in the atmospheric boundary layer wind tunnel at CPP (CPP Wind Engineering Consultants) in Colorado, USA. A generic model of an HSAT array is tested with and without the support structures (torque tube, dual-rail) for a wide range of tilts and wind directions. GC_N and GC_M for different load cases are calculated and compared between tracker systems with and without these support structures.

2 EXPERIMENTAL SETUP

2.1 *Test model*

The test model consisted of an array of 8 rows of trackers. Three rows were dummies, and 5 rows were instrumented with hundreds of pressure taps each on the top and bottom surfaces of the PV modules. The tap resolution was higher towards the exposed edge (South) of the tracker, as shown in Figure 3 for one tracker. The top taps are marked with 'O's and the bottom (underside) taps are marked with '△'s. The same HSAT model was tested with and without the support structures (torque tube, dual-rail) (Figure 4). The model included some gaps along the span and as shown by Fewless and Banks (2016), gaps affect the surface pressure at the taps close to the gap. Load cases analyzed in this study do not include any gaps within the corresponding tributary areas and therefore, taps adjacent to the gaps were not included in the analysis.

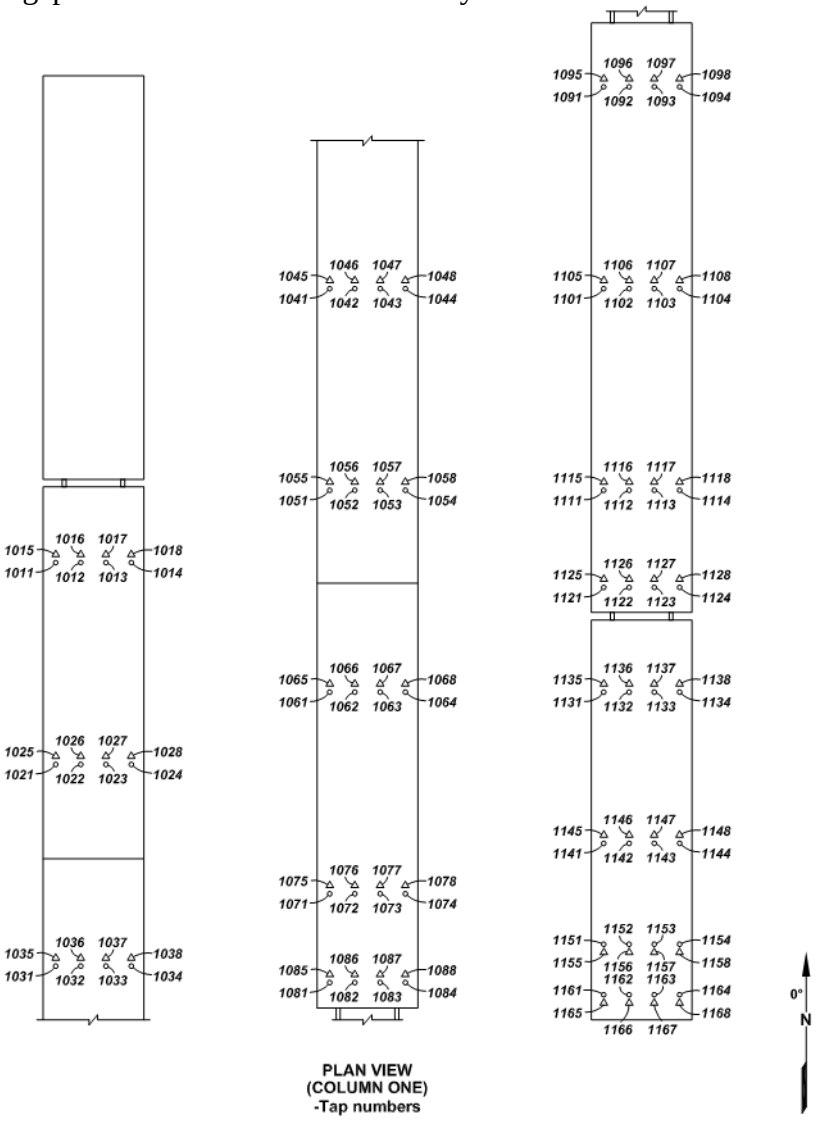

Figure 3. Tap layout on a single row

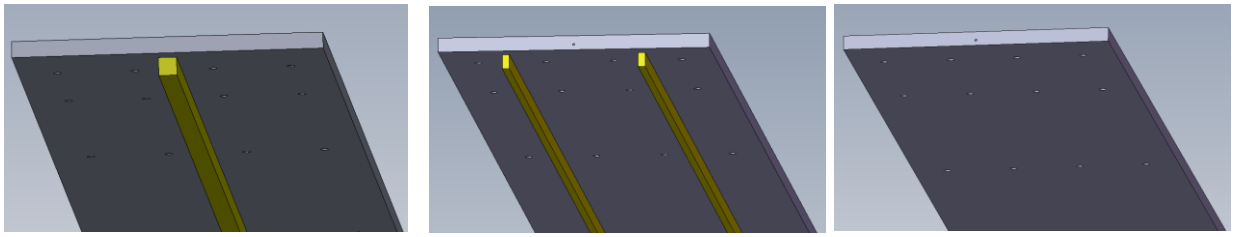

With torque tube | With dual-rail | Without torque tube or dual-rail

Figure 4. Drawings of the model with and without the support structures

2.2 *Wind tunnel facility*

Wind tunnel testing was conducted in one of CPP's boundary layer wind tunnels shown in Figure 5. The wind tunnel has a 68-ft (21-m) long test section, typically covered with roughness elements to reproduce the atmospheric wind characteristics required for the model test. A photograph of the tracker array model in the wind tunnel is shown in Figure 6.

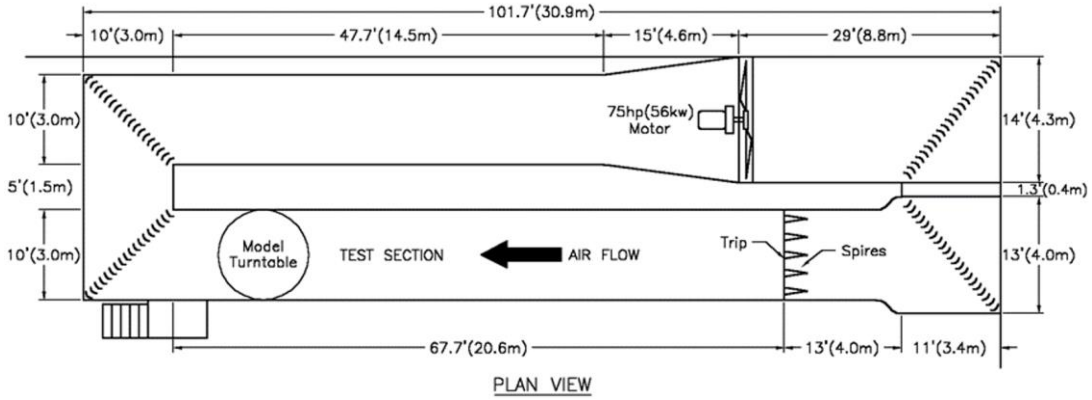

Figure 5. Schematic of the boundary layer wind tunnel

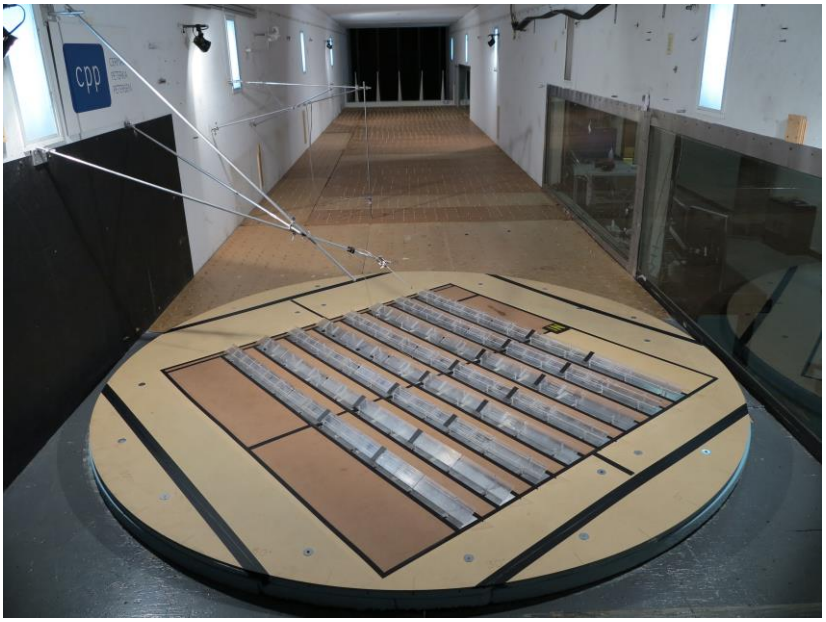

Figure 6. Setup of the model in the wind tunnel

2.3 *Test conditions*

The wind tunnel tests were conducted for open terrain (referred to as exposure C in ASCE 7). Velocity and turbulence intensity profiles as well as the spectrum of the longitudinal (alongwind) velocity adopted in the present study are provided in Figure 7. Focus was given to matching the high frequence end of the spectra. According to Richards et al. (2007), peak pressure coefficients as a ratio of peak surface pressures to peak dynamic pressures are less sensitive to spectral differences between full-scale and model-scale when high frequency end of the spectra is matched.

The tracker model was tested for a wide range of tilts. For the current study, the investigated tilts were 0°, 5°, 10°, 20°, 45°, and 60°. The model was also tested for wind azimuths of 90° (East) to 270° (West) at 10° intervals. When tilted, the models are nose-down to the east, so that east winds tend to produce downforce and west winds produce uplift.

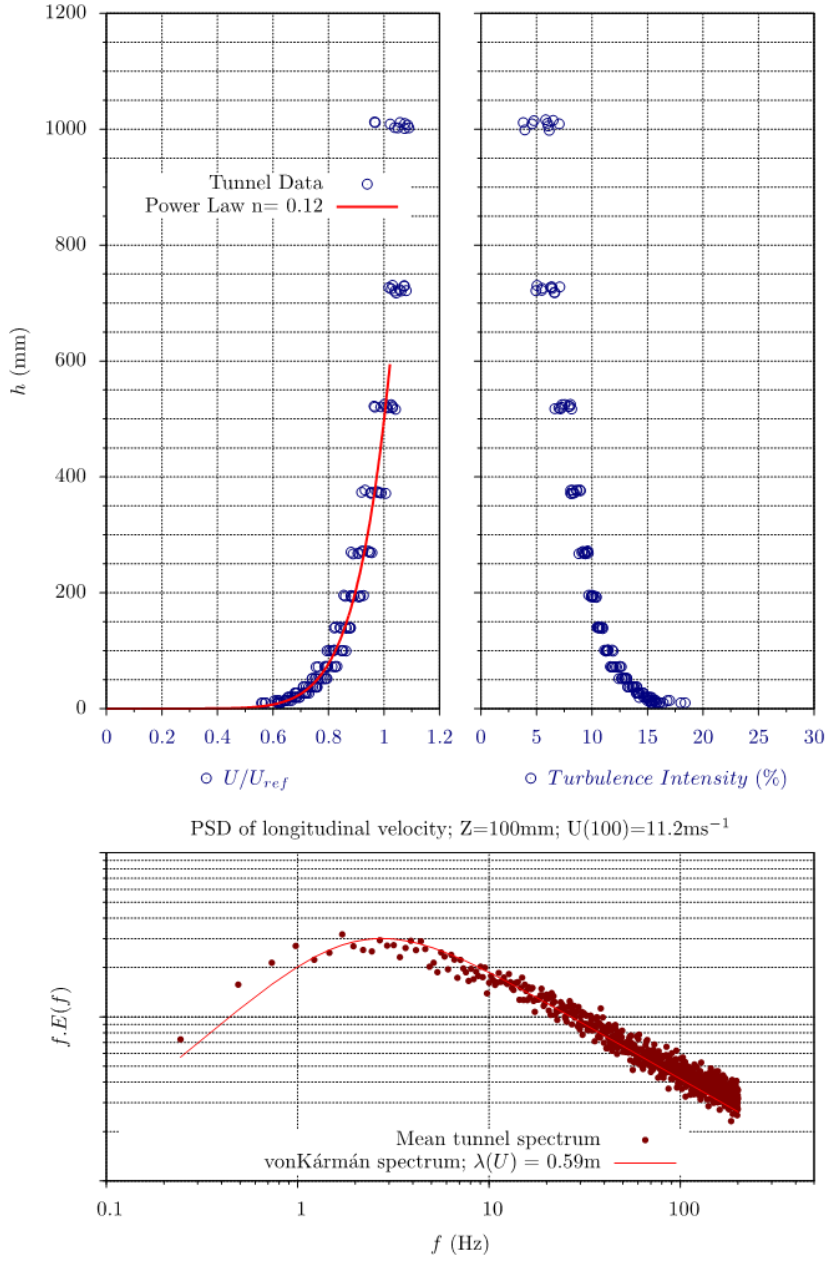

Figure 7. Velocity and turbulence intensity profiles (top), turbulence spectrum (bottom)

3 RESULTS AND DISCUSSION

3.1 *Analyzed system*

The HSAT system that has been analyzed to investigate different load cases is depicted in Figure 8. While representative, the dimensions presented in Figure 8 overall do not match any real-world trackers to the best of authors' knowledge. It is a central drive system with a chord length (L) of 2.4 m, mid-chord height of 0.55L and a ground coverage ratio (GCR = L/on-center row spacing) of 0.35. The geometric scale of the tested model for this system is 1:40.

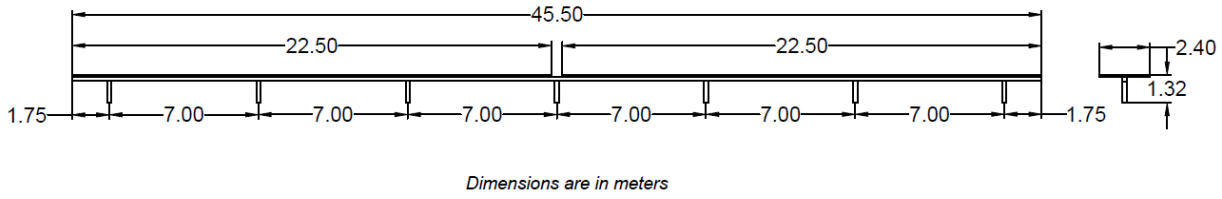

Figure 8. Tracker system used in the analysis

3.2 *Load cases*

Effects of the structures below the PV modules on three different load cases are investigated here. The load cases are tracker wing moment, post normal force and purlin moment. The tributary area of a tracker wing includes the area of all modules on half of the tracker, the tributary area of a post extends halfway to the next post in either direction along the row, and in the case of the first post it begins at the end of the row, and the tributary area of a purlin is a strip along the full length of the chord and half the width of a module on either side, which is well represented by a single tap row. Details of the torque tube and dual-rail effect on the above load cases are presented in the following sub-sections.

3.2.1 *Tracker wing moment*

Peak moment coefficients (GC_M) for a tracker wing span of 22.5 m (Figure 8) are presented in Figure 9 for a 0° tilt. As will be shown, the lower tilts are affected the most by the presence of the module underneath structures. Figure 9 shows the GC_M for the tracker wing normalized by the overall peak GC_M from all wind directions for trackers without underside support structure. Results are presented for the first windward perimeter row and one of the interior rows (5th row from the East or West edge). Only half of the wind directions tested are shown in the figure because of flow symmetry for 0° tilt.

As can be seen from Figure 9, presence of the dual-rail increased tracker wing GC_M by about 85% on the perimeter row for winds normal to the tracker axis and adding a torque tube increased this load by 40% compared to no structures underneath the panels. At the interior row, the increase was about 40% and 30% for dual-rail and torque tube respectively.

To investigate the pressure patterns related to this increase, pressure coefficients (GC_P's) at individual taps for a tap row have been plotted in Figure 10. GC_P is defined as:

$$GC_P = \frac{P}{q_Z} \tag{3}$$

where P is the surface pressure at a pressure tap. The tap row includes four taps at the top surface and the corresponding four taps at the bottom surface marked as 1161 to 1168 in Figure 3. Only the minimum GC_P on the top surface and the maximum GC_P on the bottom surface are shown in the plot as the combination of these two would result in the maximum uplift moment. Negative

GC_P is suction or pressure acting away from the panel surface (pulling up on the top surface); and positive GC_P acts toward the surface (pushing up on the underside). The location of the torque tube as well as the dual-rail are also shown in the plots using solid black lines. The leading edge of the panel is at 0 on the x-axis.

It can be clearly seen from the GC_N at the bottom taps that the coefficient is dropping downwind of the torque tube or dual-rail because of the flow separation created by these structures. Also, maximum GC_N at the taps upwind of the torque tube or dual-rail is higher than the no torque tube configuration. This could be due to the flow experiencing stagnation upwind of these structures.

While the top surface pressures are largely unchanged between the configurations, it is interesting that suction close to the leading edge on the top surface is higher for the dual-rail, with torque tube and no torque tube configurations showing similar values. This indicates that the location of these structures can affect the pressure distribution on the top surface if placed too close to the leading edge. This could be due to the flow getting obstructed by the underneath structures close to the leading edge and diverting more towards the top surface creating higher suction. Overall, the significant differences in the pressure distributions on the surfaces of the panel resulted in higher GC_M for torque tube and dual-rail that is depicted in Figure 9.

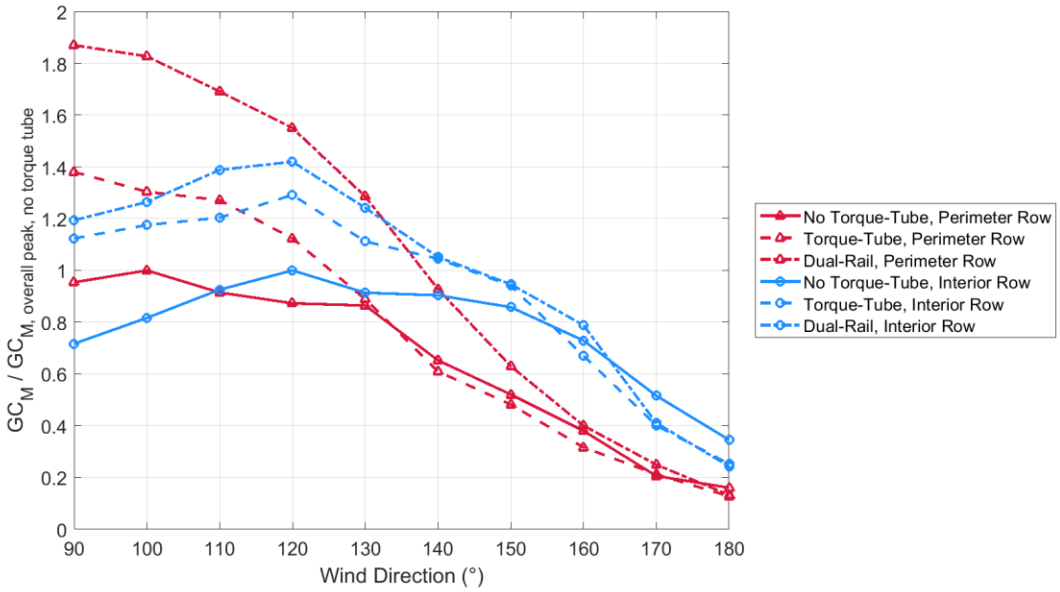

Figure 9. Ratio of GC_M between with and without panel underneath structures at 0° tilt

Ratios of GC_M with and without support structures beneath the panels are presented in Figure 11 for the perimeter and interior rows for all tilts studied herein. Three rows from the East or West exposed edge are defined as perimeter and the rest as interior. Uplift moments (from winds approaching the high side) are presented separately from downforce moments.

For perimeter uplift, the effect of the underneath structures is greatest at 0° tilt, and gradually diminishes at 10° tilt before rising slightly back up towards 45° tilt and higher. At moderate tilts (10°, 20°), wind normal to the tracker axis is found to be governing and as the underside of the panel is directly facing the wind, the effect of the underneath structures is minimal. On the other hand, at higher tilt the governing wind direction shifts towards oblique directions, where corner vortices at the end of the tracker govern the wing moment.

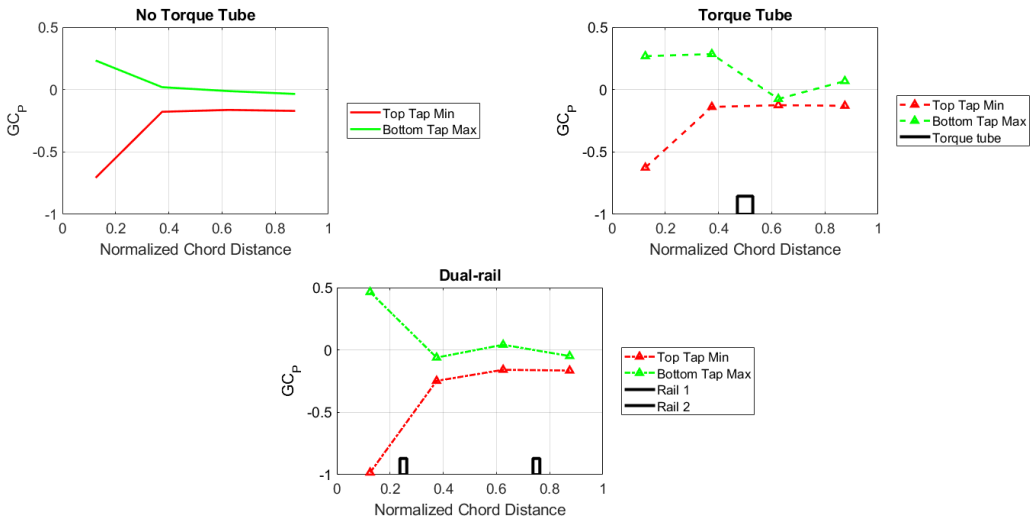

Figure 10. GC_P profiles on the top and bottom surfaces of the panel for 0° tilt. 90° wind is from left to right.

Contrary to uplift, presence of torque tube or dual rail resulted in significantly lower downforce GC_M at low tilts. Once again, we look to a representative tap row for insight. GC_P profiles at the taps 1161 to 1168 (Figure 3) for 5° tilt is plotted in Figure 12. Maximum GC_P values of the top taps and minimum GC_P values of the bottom taps are shown as the combination of these two would govern the peak downforce moment. At this tilt, suction on the underside dominates the loading, due to formation of a flow separation and reattachement along the leading edge.

Also, the suction close to the leading edge underneath the panel is higher for the configuration without any torque tube or dual-rail than with those structures. This could be due to the underneath support structures disrupting the reattachment. Although situated on the leeward side of the panel, the stagnation/wake signature of the underneath structure on the GC_P is still evident in the saw-tooth GC_P pattern of the torque tube bottom taps.

As in the uplift case, the top taps are affected more by the dual-rail than the torque tube, indicating that the position of these structures with respect to the leading edge needs to be considered while determining wind loads coefficients. As can be seen from Figure 12, the lowest net GC_N from the top and bottom taps for the dual-rail, especially at the leading edge, resulted in the lowest GC_M ratio at 5° tilt downforce at the perimeter rows among the three configurations (dual-rail, torque tube, no torque tube or dual-rail).

Fairly similar trends as the perimeter rows are observed for the interior rows in Figure 11. As interior rows do not see much shelter from perimeter rows at lower tilt, the effect of the underneath structures on GC_M is still prominent at tilts 0° to 10°. At moderate to high tilts at the interiors, complex flow interactions within different rows, with and without the underneath structures, could have resulted in the observed differences in GC_M.

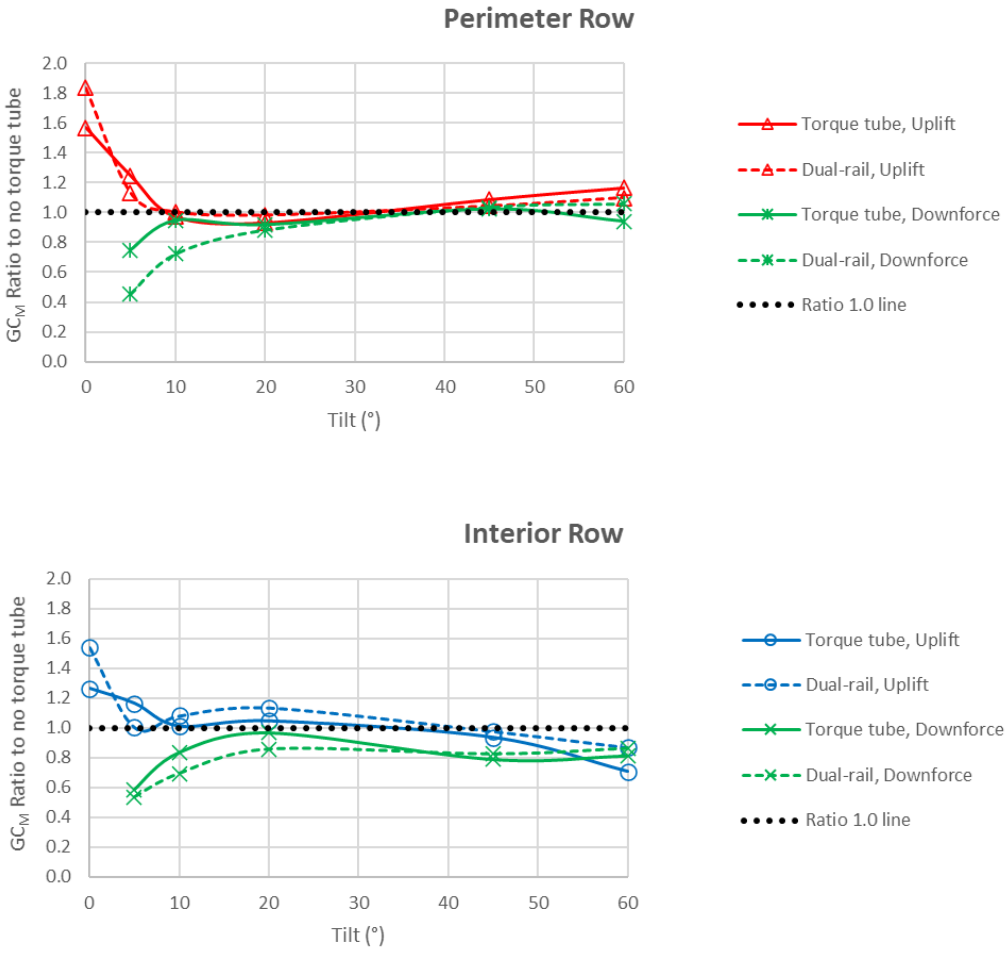

Figure 11. GC_M ratio between with and without panel underneath structures for tracker wings for a range of tilts

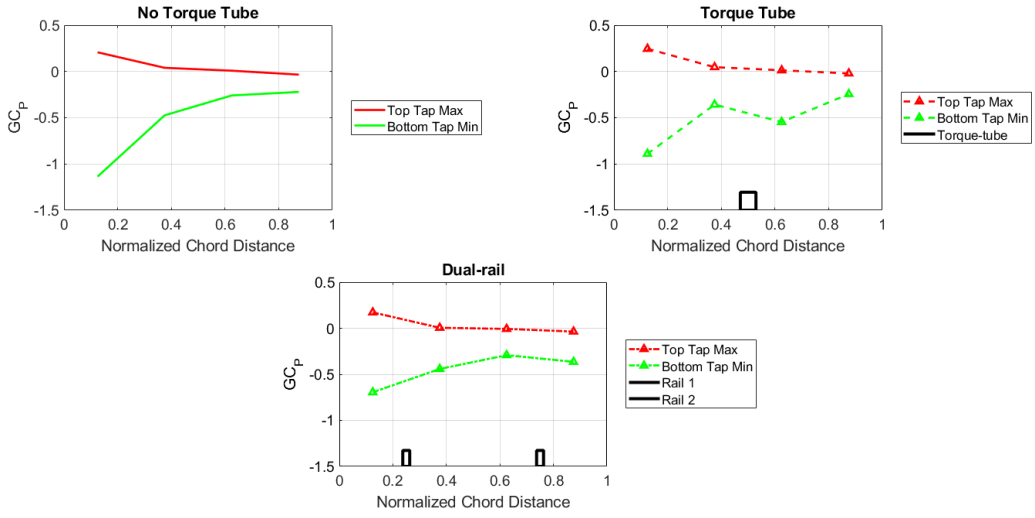

Figure 12. GC_P profiles on the top and bottom surfaces of the panel for 5° tilt

3.2.2 *Post normal force*

Peak normal force coefficient (GC_N) for a post tributary area is also calculated and analyzed. Ratios of GC_N are presented in Figure 13 for the posts in the perimeter and interior rows for all tilts studied here. Similar to GC_M, posts in the three tracker rows from the East or West exposed edge are defined as perimeter and the rest as interior.

As can be seen from Figure 13, the overall effect of the panel underneath structures on GC_N for posts are less significant than what has been observed for GC_M for tracker wings. In some cases, this is because for post normal force, the underside sawtooth pressure pattern due to stagnation and wake on either side of the support structure cancels itself out. Table 1 shows the minimum GC_P's for three rows of taps from the exposed South edge (Figure 3) on the bottom surface of the first windward row for 0° tilt and for wind coming from the East (90°). These three tap rows are within the tributary area of the first post. In Table 1, the distances along the chord from the leading edge and along the span from the South edge are normalized by the chord length. On the other hand, GC_P's are normalized by the overall minimum GC_P observed in the taps shown in Table 1. Although, the effect of the torque or dual-rail is evident in the GC_P distribution along the chord, averaging all the taps to obtain post loads washes out the effect. For tilts larger than 10°, the effect of the panel underneath structures is minimal, within about ±10% of the configuration without any torque tube or dual-rail.

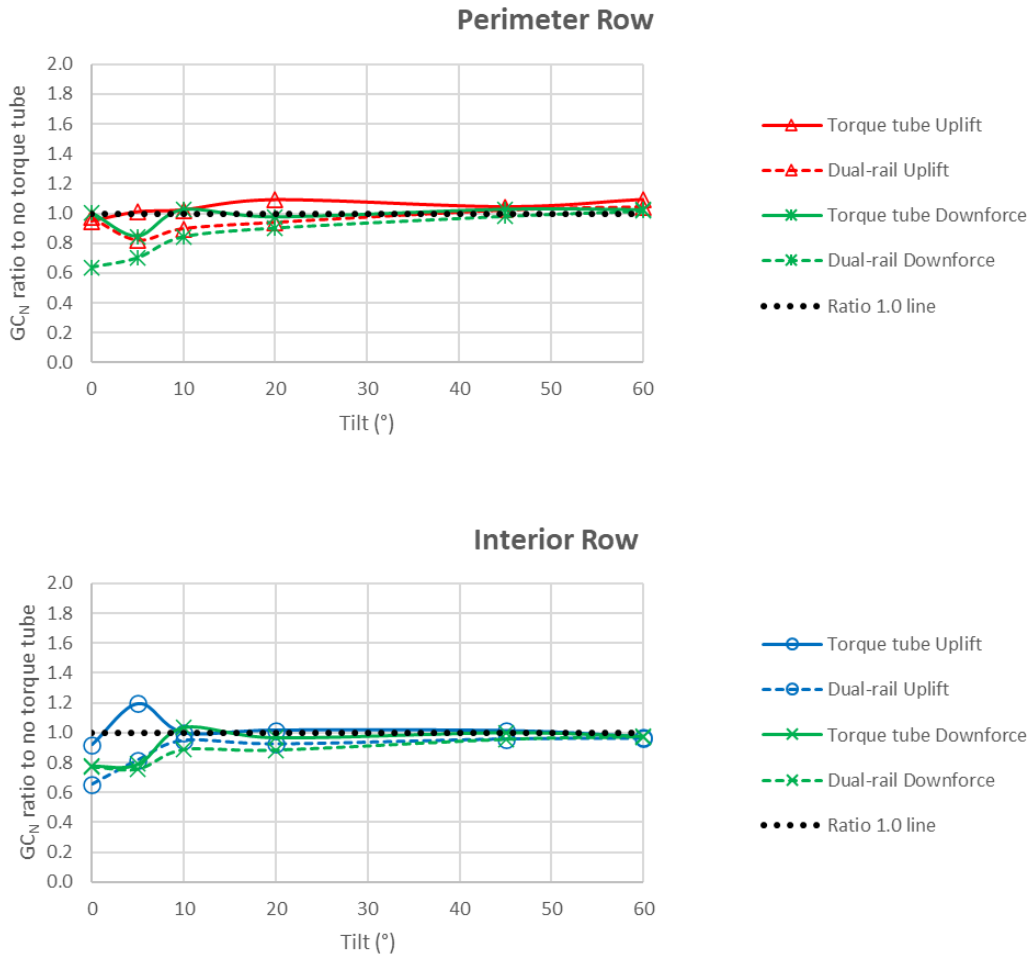

Figure 13. GC_N ratio between with and without panel underneath structures for posts for a range of tilts

Normalized distance along chord	Normalized distance along span	Normalized $GC_{P,min}$		
		No Torque Tube	Torque Tube	Dual-rail
0.9	1.8	0.3	0.4	0.4
0.6	1.8	0.3	0.7	0.4
0.3	1.8	0.3	0.1	0.5
0.1	1.8	0.8	0.7	0.3
0.9	0.7	0.3	0.4	0.4
0.6	0.7	0.2	0.7	0.4
0.3	0.7	0.3	0.2	0.5
0.1	0.7	1.0	0.9	0.4
0.9	0.2	0.2	0.3	0.3
0.6	0.2	0.2	0.6	0.4
0.3	0.2	0.2	0.2	0.4
0.1	0.2	0.9	0.8	0.5
	Averages	**0.4**	**0.5**	**0.4**

Table 1. Normalized minimum GC_P's for three rows of taps on the bottom surface

3.2.3 *Purlin moment*

To investigate the effect of panel underneath structures on a component with smaller tributary area, peak moment coefficients (GC_M) for purlins are analyzed. Figure 14 shows the GC_M ratio between with and without panel underneath structures for tilts from 0° to 60° for both at the perimeter and interior rows. Since this is a moment load case, the trend is very similar to the results obtained for GC_M tracker wing for the same reasons as outlined in Section 3.2.1. The configuration with dual-rail at 0° tilt resulted in the maximum difference for both perimeter (about 40% higher) and interior (about 50% higher) rows when compared with the configuration without any structures underneath the panel.

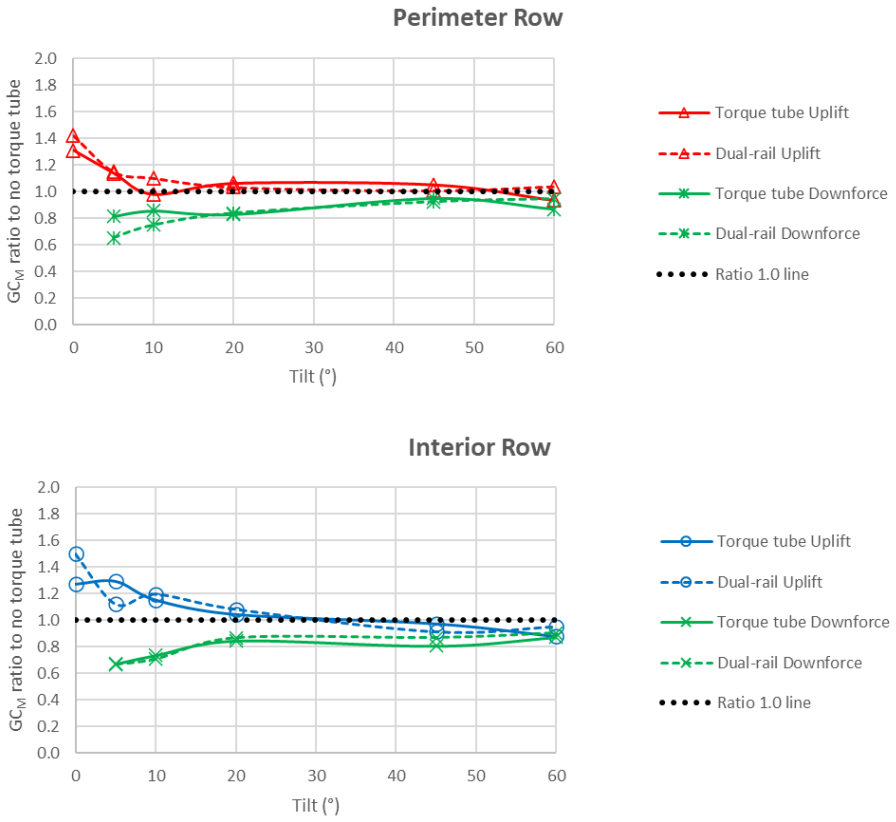

Figure 14. GC_M ratio between with and without panel underneath structures for purlins for a range of tilts

4 CONCLUSIONS

Wind tunnel tests have been conducted to investigate the effect of the structures underneath the photovoltaic (PV) panels, such as torque tube or dual-rail in horizontal single-axis trackers (HSAT), on wind induced loads. Three different load cases (tracker wing moment, post normal force and purlin moment) are analyzed for a range of tilts (0° to 60°) and wind azimuths (90° to 270°). Key observations from the study are listed below:

- Presence of the torque tube or dual-rail has a pronounced effect at 0° to 10° tilts in general for the three load cases studied herein. This is critical, because HSATs will often stow at low tilts during design wind events.
- For the tracker wing moment load case, moment coefficients with strucutures underneath the panel can be significantly higher (>50%) than those without any torque tube or dual-rail.
- Positioning of these structures with respect to the leading edge of the panel is important as this can affect the flow over the top surface of the PV panels in addition to affecting the flow underneath.
- For the post normal force load case, the effect of the underneath structures on the normal force coefficients is less significant than the tracker wing moment. The maximum increase of post normal force coefficient is found to be 1.2 times the normal force coefficient without any torque tube or dual-rail.
- For the purlin moment load case, presence of the structures underneath the PV panels increased the moment coefficients by about 40% in the perimeter rows and by 50% in the interior rows.

The above findings clearly indicate that the support structures underneath the PV panels need to be modelled for reasonable estimation of design wind loads of HSAT from wind tunnel tests. This design approach is essential for ensuring HSAT's stability and longevity.

Future studies focusing on different ground coverage ratios and ground clearances would definitely provide valuable insights towards better understanding on the effect of the support structures on wind loads. In addition, studies on the effect of these structures on dynamic loads as well as aeroelastic instability of HSATs (Rohr et al., 2015) would also be valuable.

5 REFERENCES

ASCE 7-16, 2017. Minimum Design Loads and Associated Criteria for Buildings and Other Structures, Standards. American Society of Civil Engineers.

ASCE/SEI 49-21, 2021. Wind Tunnel Testing for Building and Other Structures, Standards. American Society of Civil Engineers.

Fewless, Y., Banks, D., 2016. Challenges in wind tunnel testing of ground mount photovoltaic solar racking systems. Presented at the 8th International Colloquium on Bluff Body Aerodynamics and Applications, Northeastern University, Boston, Massachusetts, USA.

Richards, P.J., Hoxey, R.P., Connell, B.D., Lander, D.P., 2007. Wind-tunnel modelling of the Silsoe Cube. J. Wind Eng. Ind. Aerodyn., The Fourth European and African Conference on Wind Engineering 95, 1384–1399. https://doi.org/10.1016/j.jweia.2007.02.005

Rohr, C., Bourke, P.A., Banks, D., 2015. Torsional Instability of Single-Axis Solar Tracking Systems. Presented at the 14th International Conference on Wind Engineering, Porto Alegre, Brazil.